Published online 12 September 2022

Nucleic Acids Research, 2022, Vol. 50, No. 17 ***9765–9779***
https://doi.org/10.1093/nar/gkac735

Mitochondrial stress induces AREG expression and epigenomic remodeling through c-JUN and YAP-mediated enhancer activation

Yuko Hino[1], Katsuya Nagaoka[1], Shinya Oki[2], Kan Etoh[1], Shinjiro Hino[1,*] and Mitsuyoshi Nakao[1,*]

[1]Department of Medical Cell Biology, Institute of Molecular Embryology and Genetics, Kumamoto University, Kumamoto 860-0811, Japan and [2]Department of Drug Discovery Medicine, Kyoto University Graduate School of Medicine, Kyoto 606-8507, Japan

Received May 02, 2022; Revised August 08, 2022; Editorial Decision August 11, 2022; Accepted August 19, 2022

ABSTRACT

Nucleus–mitochondria crosstalk is essential for cellular and organismal homeostasis. Although anterograde (nucleus-to-mitochondria) pathways have been well characterized, retrograde (mitochondria-to-nucleus) pathways remain to be clarified. Here, we found that mitochondrial dysfunction triggered a retrograde signaling via unique transcriptional and chromatin factors in hepatic cells. Our transcriptomic analysis revealed that the loss of mitochondrial transcription factor A led to mitochondrial dysfunction and dramatically induced expression of amphiregulin (*AREG*) and other secretory protein genes. *AREG* expression was also induced by various mitochondria stressors and was upregulated in murine liver injury models, suggesting that *AREG* expression is a hallmark of mitochondrial damage. Using epigenomic and informatic approaches, we identified that mitochondrial dysfunction-responsive enhancers of *AREG* gene were activated by c-JUN/YAP1/TEAD axis and were repressed by chromatin remodeler BRG1. Furthermore, while mitochondrial dysfunction-activated enhancers were enriched with JUN and TEAD binding motifs, the repressed enhancers possessed the binding motifs for hepatocyte nuclear factor 4α, suggesting that both stress responsible and cell type-specific enhancers were reprogrammed. Our study revealed that c-JUN and YAP1-mediated enhancer activation shapes the mitochondrial stress-responsive phenotype, which may shift from metabolism to stress adaptation including protein secretion under such stressed conditions.

GRAPHICAL ABSTRACT

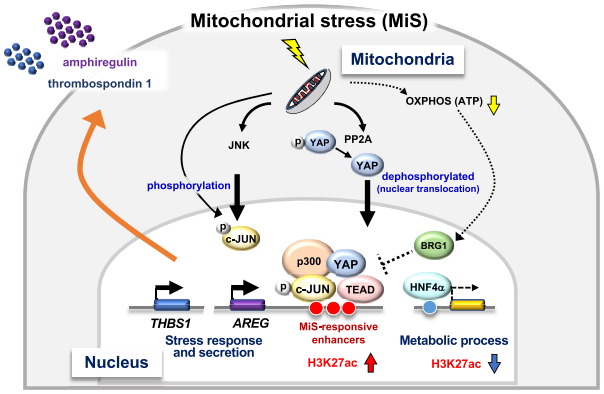

INTRODUCTION

Nucleus–mitochondria crosstalk is essential for cell maintenance and environmental responses (1). While mitochondria rely most of their function on nuclear genome-encoded proteins, mitochondria supplies the nucleus with metabolites such as acetyl-CoA and S-adenosylmethionine, which are essential for DNA and histone modifications (2,3). Thus, cells need to regulate both anterograde (nucleus-to-mitochondria) and retrograde (mitochondria-to-nucleus) pathways in a highly ordered manner to properly maintain cell function.

In the anterograde pathway, nuclear transcription factors such as peroxisome proliferator-activated receptor-γ coactivator-1α (PGC-1α) and nuclear respiratory factor 1 (NRF1) promote the expression of mitochondria-related genes including *mitochondrial transcription factor A* (*TFAM*), which plays a pivotal role in regulating transcription, replication and organization of the mitochondrial genome (4–6). Therefore, TFAM is involved in metabolic

*To whom correspondence should be addressed. Tel: +81 96 373 6800; Fax: +81 96 373 6804; Email: mnakao@gpo.kumamoto-u.ac.jp
Correspondence may also be addressed to Shinjiro Hino. Tel: +81 96 373 6801; Fax: +81 96 373 6804; Email: s-hino@kumamoto-u.ac.jp

© The Author(s) 2022. Published by Oxford University Press on behalf of Nucleic Acids Research.
This is an Open Access article distributed under the terms of the Creative Commons Attribution-NonCommercial License (http://creativecommons.org/licenses/by-nc/4.0/), which permits non-commercial re-use, distribution, and reproduction in any medium, provided the original work is properly cited. For commercial re-use, please contact journals.permissions@oup.com

activities in the mitochondria as an essential regulator between cellular organelles. In addition, chromatin regulators in the nucleus significantly contribute to mitochondrial functions. For example, lysine specific demethylase-1 (LSD1) inhibits oxidative phosphorylation (OXPHOS) and fatty acid oxidation by repressing the *PGC-1α* gene via flavin adenine dinucleotide (FAD)-dependent demethylation of histone H3 at lysine 4 (7,8). SETD8 (also known as PR-Set7) protects cellular senescence by limiting protein synthesis and energy metabolism through the monomethylation of histone H4 at lysine 20 (9). These previous studies have established that mitochondrial function is controlled by the nuclear factors (10,11).

Mitochondria are important regulators of a variety of metabolites, including acetyl-CoA, S-adenosylmethionine, ATP, NAD^+/NADH, FAD/$FADH_2$ and second messengers such as free calcium and reactive oxygen species in mammalian cells (1,3). Because the production of these metabolites is influenced by mitochondria damage, they directly or indirectly constitute the retrograde pathway, also known as mitochondrial stress signaling. In addition, some transcription factors/cofactors such as SIRT3 contribute to retrograde signaling (12,13). Recently, G-protein pathway suppressor 2 (GPS2) was found to mediate the retrograde pathway via the mitochondria-to-nucleus translocation (14). However, not much is known about how damaged mitochondria transfer their signal to the nuclear machinery and change gene expression. In particular, mechanisms by which retrograde signal can induce specific epigenomic changes at specific loci remain unclear.

Human cases and mouse models of non-alcoholic fatty liver disease (NAFLD) and non-alcoholic steatohepatitis (NASH) are associated with fat accumulation in the liver, mitochondrial dysfunction and cellular senescence in hepatocytes (15–18). These chronic fatty liver conditions widely affect the global adult population and are potentially severe because of the increased risk of metabolic syndrome and the development of hepatocellular carcinoma. Although mitochondrial stresses play crucial roles in disease development, it is unclear whether abnormal crosstalk between the nucleus and mitochondria coexists with NAFLD/NASH pathophysiology.

In this study, we identified a TFAM depletion-induced retrograde pathway that involves multiple signaling and transcription factors in hepatic cells. Our data reveal the molecular mechanism of mitochondrial stress-induced phenotype, which might explain how cells adapt and survive under stressful conditions.

MARERIALS AND METHODS

Cell culture

HepG2 cells were purchased from the Japanese Collection of Research Bioresources (JCRB) Cell Bank and cultured in Dulbecco's modified Eagle's medium (DMEM)-high glucose (Sigma) supplemented with 10% (v/v) heat-inactivated fetal bovine serum (FBS) and penicillin/streptomycin (P/S). HeLa cells (JCRB) were cultured in DMEM/F-12 Ham medium (Sigma) supplemented with 10% FBS and P/S. IMR90 cells (ATCC) were cultured in Eagle's minimum essential medium with Earle (Sigma) supplemented with 200 mM L-glutamine, 10% FBS, and P/S. To establish ρ0 cells, HepG2 cells were cultured in the above-mentioned DMEM-high glucose containing 1 μg/ml ethidium bromide, 100 μg/ml sodium pyruvate and 50 μg/ml uridine for 10 days (19). Mitochondrial DNA (mtDNA) was extracted using DNAzol Reagent (Thermo Fisher Scientific), and the tRNA-Leu and β2 microglobulin contents were quantified by quantitative real-time PCR. The amount of mtDNA was calculated using the tRNA-Leu/β2 microglobulin (20). For inhibition of oxidative phosphorylation, HepG2 cells were treated with 0.5 μg/ml of oligomycin (O4876, Sigma) for 24 h. For the knockdown experiments, siRNAs were transfected using Lipofectamine RNAiMAX Transfection Reagent (Thermo Fisher Scientific) according to the manufacturer's protocol. For c-JUN knockdown, siGENOME Human JUN siRNA SMARTpool (Dharmacon) was used. Target sequences of siRNAs are listed in Supplementary Table S1. Unless otherwise stated, knockdown experiments were conducted after 72 h. An inhibitor of the c-JUN N-terminal kinase (JNK), SP600125 (420119, Sigma-Aldrich), was added to the medium at the indicated concentrations until 4–72 h after siRNA transfection.

Antibodies

For immunofluorescence, western blot analysis or ChIP-qPCR, the following antibodies were used in these experiments: TFAM (ab89818 or ab176558, Abcam), amphiregulin (AF262, R&D Systems), beta tubulin (66240–1-Ig, Proteintech), c-JUN (H-79) (sc-1694, Santa Cruz Biotechnology) or c-JUN (G-4) (sc-74543), phospho-c-Jun (Ser73) (D47G9) XP rabbit mAb (#3270, Cell Signaling Technology), YAP/TAZ (D24E4) (#8418) or YAP (D8H1X) XP® rabbit mAb (#14074), phospho-YAP (Ser127) (D9W2I) rabbit mAb (#13008), purified mouse anti-TEF-1 (610923, BD Biosciences), TFIID (TBP) (58C9) (sc-421), BRG-1 (G-7) (sc-17796), anti-FLAG M2 monoclonal, affinity purified (F1804, Sigma-Aldrich), anti-histone H3 (mono methyl K4) - ChIP grade (ab8895) or anti-histone H3 (acetyl K27) - ChIP grade (ab4729).

Transcriptome analysis

Genome-wide expression analysis was conducted using the Affymetrix GeneChip Human Genome U133 Plus 2.0 Array. mRNA from HepG2 and HeLa cells was extracted using the RNeasy Mini Kit (QIAGEN), and cDNA synthesis, cRNA amplification, hybridization and scanning were provided by Takara Bio Inc. The raw data were normalized with the MAS5 algorithm, and data annotation analysis was conducted using the GeneSpring GX software (Agilent). The GeneChip array data have been deposited in the GEO under ID codes GSE196511. In addition, HNF4α-regulated genes were analyzed using the expression array data from HNF4α-KD HepG2 cells (GSE29084) (21). The raw data were normalized using the RMA algorithm.

Quantitative RT-PCR

Total RNA was extracted from cells using TRIzol reagent (Thermo Fisher Scientific). Complementary DNA was syn-

thesized using ReverTra Ace qPCR RT Master Mix or ReverTra Ace qPCR RT Master Mix with gDNA Remover (TOYOBO). Relative gene expression was quantified using THUNDERBIRD SYBR qPCR Mix or THUNDERBIRD Next SYBR qPCR Mix (TOYOBO) reagent and StepOnePlus or QuantStudio 3 Real Time PCR System (Thermo Fisher Scientific). Fold changes were determined using the 2-ΔΔCt method, and were calculated as the difference between the experimental and the respective control groups. Primer sequences are listed in Supplementary Table S2.

Immunofluorescence

Immunofluorescence of the cell lines was conducted as previously described (22). Briefly, cells were fixed with 4% paraformaldehyde in phosphate-buffered saline (PBS) for 15 min at room temperature, washed with PBS, permeabilized with 0.2% Triton X-100 and 0.5% BSA in PBS for 5 min on ice, blocked with 0.5% bovine serum albumin in PBS, incubated with specific primary antibodies for 1 h at room temperature or overnight at 4°C, and then incubated with appropriate fluorescent-labeled secondary antibodies for 1 h at room temperature. The cells were counterstained with DAPI (1 μg/ml) before mounting. Images were obtained with a microscope IX-71 (Olympus) and the image acquisition software Lumina Vision Version 2.4 (Mitani).

Western blot analysis

At 72 h after siRNA transfection, cells were washed in PBS and lysed with ice-cold RIPA buffer (50 mM Tris-HCl pH 8.0, 150 mM NaCl, 1 mM EDTA, 1% (v/v) Triton X-100, 0.1% SDS, 0.1% sodium deoxycholate) supplemented with a protease inhibitor and phosphatase inhibitor cocktails (Nacalai Tesque). For AREG detection, cells were treated with 5 μg/ml brefeldin A (022–15991, FUJIFILM Wako Chemicals)-containing medium for 6 h prior to harvesting. Lysates were subjected to SDS–PAGE, followed by immunoblotting using the Trans-Blot Turbo Transfer System (Bio-Rad). Membranes were blocked with 5% skim milk and 0.3% Tween20 in PBS for 30 min at room temperature, incubated with primary antibody overnight at 4°C, and incubated with horseradish peroxidase-labeled secondary antibody for 1 h at room temperature. ECL Prime western blotting Detection Reagent (GE Healthcare) or Western Lightning Plus-ECL (PerkinElmer Japan) were used as the substrate. Band detection and quantification were conducted using ImageQuant LAS 4000 and ImageQuant TL (GE Healthcare).

Luciferase vector construction

To construct the pGL4.15-RE-AREG promoter, the *Bam*HI-*Sal*I fragment containing the SV40 early enhancer/promoter was deleted from pGL4.15. Additionally, 2.3 kb of the *AREG* promoter, amplified by PCR from the HepG2 genome, was inserted into the *Hind*III site. RE1, RE2 or RE3 fragments were also amplified from the HepG2 genome and inserted into the *Nhe*I-*Bgl*II site. The primers, amplicon size and restriction enzyme sites at both ends were as follows:

RE 1; RE 1_EcoRV-F, RE 1_BglII-R, 1.3 kb, *Eco*RV and *Bgl*II

RE 2; RE 2_XhoI-F, RE 2_EcoRV-R, 0.5 kb, *Xho*I and *Eco*RV

RE 3; RE 3_NheI-F, RE 3_XhoI-R5, 0.5 kb, *Nhe*I and *Xho*I

Luciferase reporter assay

Luciferase reporter analyses were conducted using a dual-luciferase reporter assay system (Promega) following the manufacturer's protocol. For *AREG* enhancer analysis, the pGL4.15-RE-AREG promoter reporter vector was co-transfected with the reference vector pGL4.74[hRluc/TK] into the HepG2 cells. After 48 h of culture, the cells were collected for luciferase measurements. Data are presented as mean ± SD. Tukey's honestly significant difference test was conducted with a significance level of 0.05, using JMP 14 software (SAS).

Cytoplasmic and nuclear extraction

Trypsinized cells were resuspended in nuclear extraction buffer (5 mM PIPES, pH 8.0, 85 mM KCl, 0.5% NP-40) supplemented with protease inhibitor cocktail and phosphatase inhibitor cocktail (Nacalai Tesque) by pipetting. After incubation on ice for 10 min, the cells were centrifuged at 830 × *g* for 5 min, and the supernatant was collected as the cytoplasmic fraction. The pellet was washed with ice-cold wash buffer (20 mM Tris-HCl, pH 7.5, 150 mM NaCl, 1 mM EDTA, 1 mM EGTA) containing protease or phosphatase inhibitor cocktail, then resuspended in 2× sample buffer, centrifuged at 18 000 × *g* for 10 min at 4°C, and the supernatant was collected as the nuclear fraction.

Lentiviral transduction

To generate the CSII-EF-3xFLAG-IRES2-Bsd mock vector, the IRES2-Bsd fragment from CSII-CMV-MCS-IRES2-Bsd (RDB04385, RIKEN BRC DNA BANK) and an oligo with *Xho*I and *Eco*RI sites, added to both ends of the 3xFLAG sequence, were inserted into the *Bam*HI-*Xba*I sites of CSII-EF-MCS (RDB04378). For overexpression of c-JUN, CSII-EF-3xFLAG-c-JUN-IRES2-Bsd was generated by inserting a 1 kb PCR amplicon from HepG2 cDNA into the *Eco*RI-*Bam*HI sites of CSII-EF-3xFLAG-IRES2-Bsd. The PCR primers used were c-JUN_EcoRI-F and c-JUN_BamHI-R. For overexpression of YAP1 or YAP1(S127A) mutant, 1.5 kb fragments were amplified by PCR from p2xFlag CMV2-YAP2 (#19045, Addgene) or p2xFlag CMV2-YAP2-S127A mutant (#19050, Addgene) using YAP1_EcoRI-F and YAP1_NotI-R. Amplicons (1.5 kb) were inserted into the *Eco*RI-*Not*I sites of CSII-EF-3xFLAG-IRES2-Bsd. Primer sequences are listed in Supplementary Table S2. Each plasmid was co-transfected with pCAG-HIVgp (RDB04394) and pCMV-VSV-G-RSV-Rev (RDB04393) into the Lenti-X 293T cells (Takara Bio). After 48 h, the supernatant containing the virus was collected, filtered, and infected with HepG2 cells in the presence of 8 μg/ml polybrene. Infected cells were selected with 3 μg/ml blasticidin S (029–18701, FUJIFILM Wako

Chemicals). For co-expression of c-JUN and YAP1, HepG2 cell lines established by mock, YAP1, or YAP1(S127A) lentivirus infection were infected with the c-JUN virus for 48 h.

Chromatin immunoprecipitation (ChIP)-qPCR

ChIP experiments for detecting modified histones were conducted as previously described (8). Briefly, cells were crosslinked with 1% formaldehyde for 10 min at room temperature. Following cell lysis, cells were sonicated by Picoruptor (Diagenode) for 10 min or treated with 10 U of Micrococcal nuclease per 1×10^6 nuclei at 37°C for 20 min. Chromatin fragments were incubated at 4°C overnight with the appropriate antibodies, followed by a pull-down assay using protein A/G-conjugated beads. Purified DNA was subjected to quantitative PCR (qPCR) using the primer sets listed in Supplementary Table S2. For ChIPs targeting transcription factors, Dynabeads M-280 sheep anti-rabbit or anti-mouse IgG (Thermo Fisher Scientific) were used for pull-down.

ChIP-seq analysis

For ChIP-seq analyses, 5×10^6 HepG2 cells per immunoprecipitation (IP) were collected 72 h after siRNA transfection. Crosslinking and fragmentation were conducted as described for the ChIP-qPCR. Chromatin fragments were incubated at 4°C overnight with 2 μg of appropriate antibodies and immunoprecipitated with Dynabeads protein A/G (Life Technologies). After decrosslinking, the DNA was purified using a QIAquick PCR Purification Kit (Qiagen). The ChIP-seq library was prepared using a NEBNext Ultra DNA Library Prep Kit and sequenced using the Illumina NextSeq 500/550 system (Illumina), according to the manufacturer's protocol. The sequenced reads were mapped to the human reference genome (hg19) using the Burrows-Wheeler alignment algorithm with default parameters (23). Peak detection was performed using the MACS2 algorithm with an FDR cutoff value of 0.05, a composite broad region option (24), and selected peaks of enrichment greater than five times the control KD. The ChIP-seq data have been deposited in the GEO under ID codes GSE197242.

Transcription factors co-localized with the modified active enhancer mark regions were predicted using ChIP-Atlas (25) and the ChIP-seq data for c-JUN (GSM1700784) (26), YAP1 (GSM1614029) (27) and HNF4α (GSM469863) (28) were used for subsequent analyses. Peak annotations and motifs were analyzed using Homer (29), and the co-localization of ChIP-seq data was visualized using the compute matrix of deep tools (30). Functional enrichment analysis was conducted using clusterProfiler (31,32) with an FDR cutoff of 0.05. The results were visualized via dot plot or gene concept-network (cnet) plot.

For analyzing the active enhancer mark and transcription factor enrichment on enhancer regions of secretory protein genes induced by mitochondrial stress, enhancers of the genes were predicted using GeneHancer (33). ChIP-seq data of TFAM-depleted HepG2 cells, c-JUN (GSM1700784), YAP1 (GSM1614029) and TEAD1 (GSM1667161) were integrated using the Integrative Genomics Viewer (34).

Data analysis of murine NAFLD/NASH model

To analyze the *in vivo* mitochondrial stress in mice, RT-qPCR was conducted using liver samples. For the NAFLD model, 7-week-old male C57BL/6J mice were fed with normal-diet (ND), high-fat diet (HFD), or methionine and choline-deficient (MCD) diet for 4 weeks (35). For the NASH model, we reanalyzed the transcriptome dataset GSE137449 (36). Briefly, row count data obtained from RNA sequences in the liver of wild-type (WT) mice treated with ND or a choline-deficient L-amino acid-defined HFD (CDAHFD) were normalized using Deseq2 (37). Equality of variance was examined using with a significance level of 0.05.

Real-time measurement of OXPHOS activity

Cellular OXPHOS activity was monitored in real time using the XF24 Extracellular Flux Analyzer (Seahorse Bioscience), according to the manufacturer's instructions. HepG2 or HeLa cells were transfected with siRNAs 3 days prior to the assay, and 5×10^4 or 4×10^4 cells per well of HepG2 or HeLa cells were seeded on the Seahorse assay plate a day before the assay. The maximum OXPHOS capacity was determined as described previously (8).

Determination of intracellular ATP

To determine intracellular ATP concentrations, HepG2 cells were collected 48 h after siRNA transfection. ATP concentrations were determined using an ATP Bioluminescence Assay Kit CLS II (Roche), according to the manufacturer's instructions. ATP concentrations were normalized to the number of cells in the same samples.

Formaldehyde-assisted isolation of regulatory elements (FAIRE)-qPCR

FAIRE experiments to detect open chromatin sites were conducted according to a previously published protocol (38). Briefly, 9×10^5 HepG2 cells were seeded the day before siRNA transfection, and the cells were harvested 24 h after transfection. Cells were crosslinked with 1% formaldehyde for 10 min at room temperature, and after cell lysis, the DNA was sheared using a Bioruptor (Diagenode) for 10 min. The samples were de-crosslinked by overnight incubation at 65°C and purified by ethanol precipitation. The samples were subsequently treated with RNase A, purified using a QIAquick PCR purification kit (Qiagen), and used for qPCR analysis. The primer sets are listed in Supplementary Table S2.

Identification of super-enhancers

Super-enhancers were identified by Homer's findPeaks tool based on the algorithm of Whyte *et al.* (39) using acetylated H3K27 peak data from control- and TFAM-knockdown HepG2 cells.

Analysis of genome-wide long-range interactions

To analyze the interaction of RE sites and distal genomic regions, we used ChromContact, a web tool to utilize the

information obtained by Hi-C (40). Regions that interact with RE1, RE2 or RE3 were examined in AREG-expressing (NHEK, HMEC) and non-AREG-expressing (IMR90, HUVEC) cells at a resolution of 5 kb.

RNA sequencing data analysis of human NAFLD patients

Transcriptome data (GSE160016) from the livers of donors who underwent organ donation after cardiac death (6 non-NAFLD donors and 5 NAFLD donors) (41) were reanalyzed as human controls and mitochondrial stress conditions, respectively.

Motif Analysis of c-JUN and TEAD1

Potential binding sequences of AP-1 and TEAD (TEA domain transcription factor) near the RE1, RE2, and RE3 sites were predicted with MatInspector (http://www.genomatix.de) (42).

Definition of secretory protein

The 2641 genes predicted by The Human Protein Atlas (HPA) (www.proteinatlas.org) (43) according to the definition of 'all ensemble genes with at least one predicted secretory transcript' were used as secretory proteins.

RESULTS

Elevated expression of AREG is a hallmark of mitochondrial dysfunction

TFAM is a nuclear-encoded protein and indispensable for the function of mitochondrial genome. To understand the nuclear response against mitochondrial dysfunction (Figure 1A), we conducted transcriptome analyses in cultured human cells (HepG2 and HeLa) under TFAM knockdown (KD), using two siRNAs against the coding and 3′-untranslated sequences of *TFAM* mRNA (Supplementary Figure S1A). Under TFAM-KD for 72 h, both oxidative phosphorylation (OXPHOS) and glycolytic activities decreased, together with a reduction in intracellular ATP levels (Supplementary Figure S1B,C), indicating that metabolic dysfunction occurred in mitochondria. We found that 52 nuclear genes were commonly upregulated by ≥1.5-fold by TFAM-KD, while 23 genes were downregulated (Figure 1B and Supplementary Table S3). Among the genes upregulated by TFAM-KD, *Amphiregulin* (*AREG*) showed the highest induction ratio (Figure 1C), in addition to an enrichment of secretory protein genes such as *thrombospondin-1* (*THBS1*) and *CD44. AREG* upregulation was verified by quantitative RT-PCR analyses (Figure 1D,E). We also found a dramatic increase of *AREG* expression in diploid fibroblast IMR90 under TFAM-KD (Figure 1E). By immunostaining analysis, we confirmed that the AREG protein was abundantly expressed in TFAM-KD cells (Figure 1F). Intracellular AREG in TFAM-KD cells was increased by the treatment with brefeldin A (BFA), an ER-Golgi trafficking inhibitor (Figure 1G), indicating that AREG was actively secreted. Notably, *AREG* upregulation was also found under two different mitochondrial stresses in HepG2 cells, OXPHOS inhibition by oligomycin treatment and mtDNA depletion (rho0 or ρ0 state) by long-term ethidium bromide treatment (Figure 1H,I). These data indicated that the induced expression of AREG is a hallmark of mitochondrial dysfunction, and thus a key target of the retrograde signaling.

Tfam downregulation and *Areg* upregulation in mouse liver tissues under mitochondrial stress

We then investigated whether the expression of *TFAM* and *AREG* are altered under mitochondrial stress conditions *in vivo*. When fed a high-fat diet (HFD) combined with methionine and choline deficiency (HFD/MCD), mice developed liver injury due to mitochondrial damage (44). By comparing the transcriptome profile of HFD/MCD-fed mouse liver with that of normal diet (ND)-fed mice (35), we found a clear downregulation of *Tfam* expression in the HFD/MCD mice, together with a significant inverse correlation with that of *Areg* ($P < 0.01$) (Figure 2A). Next, we analyzed the transcriptome dataset from another liver injury model, in which mice were fed either ND or L-amino acid-defined/choline-deficient HFD (CD) (36). In comparison with the ND-fed mice, *Areg* and other TFAM-KD induced genes (Figure 1C), including *Thbs1* and *Cd44*, were significantly increased in the CD mice, in the presence of a decrease in *Tfam* expression (Figure 2B and Supplementary Figure S2A). In addition to mouse liver injury model, we evaluated human transcriptome datasets of liver specimens from non-alcoholic fatty liver disease (NAFLD) and non-NAFLD groups (41). *AREG* and *TFAM* transcripts tended to increase and decrease in the NAFLD group, respectively, in comparison with the non-NAFLD group (Supplementary Figure S2B). Collectively, the data suggest that the induction of *Areg* is a hallmark of liver injury, in which TFAM is inactivated.

Unique transcriptional regulators act on *AREG* gene enhancers under mitochondrial stress

Two tandem *AREG* genes, separated by a 170 kb-genomic sequence, are located within the EGF family gene cluster at human chromosome 4q13.3 (45) (Figure 3A). To evaluate the impact of mitochondrial dysfunction on the epigenome in HepG2 cells, we performed chromatin immunoprecipitation-sequencing (ChIP-seq) of monomethylated H3K4 (H3K4me1) and acetylated H3K27 (H3K27ac), which are histone marks characteristic of enhancer activity (46,47). Based on the enrichment of these active enhancer marks by TFAM-KD, we identified three putative regulatory elements (REs) between *AREG* and *betacellulin* (*BTC*) genes, named RE1, RE2 and RE3, in this region (Figure 3A). Consistent with the upregulation of the *AREG* gene, TFAM-KD elevated the levels of both H3K4me1 and H3K27ac at these sites (Figure 3B). Further, these RE1-3 sites were selectively detected as a super-enhancer that showed the accumulation of H3K4me1 and H3K27ac in TFAM-KD cells (Supplementary Figure S3A). Because enhancer activation is often accompanied by chromatin opening, we performed a FAIRE-quantitative PCR to analyze the chromatin structure around the

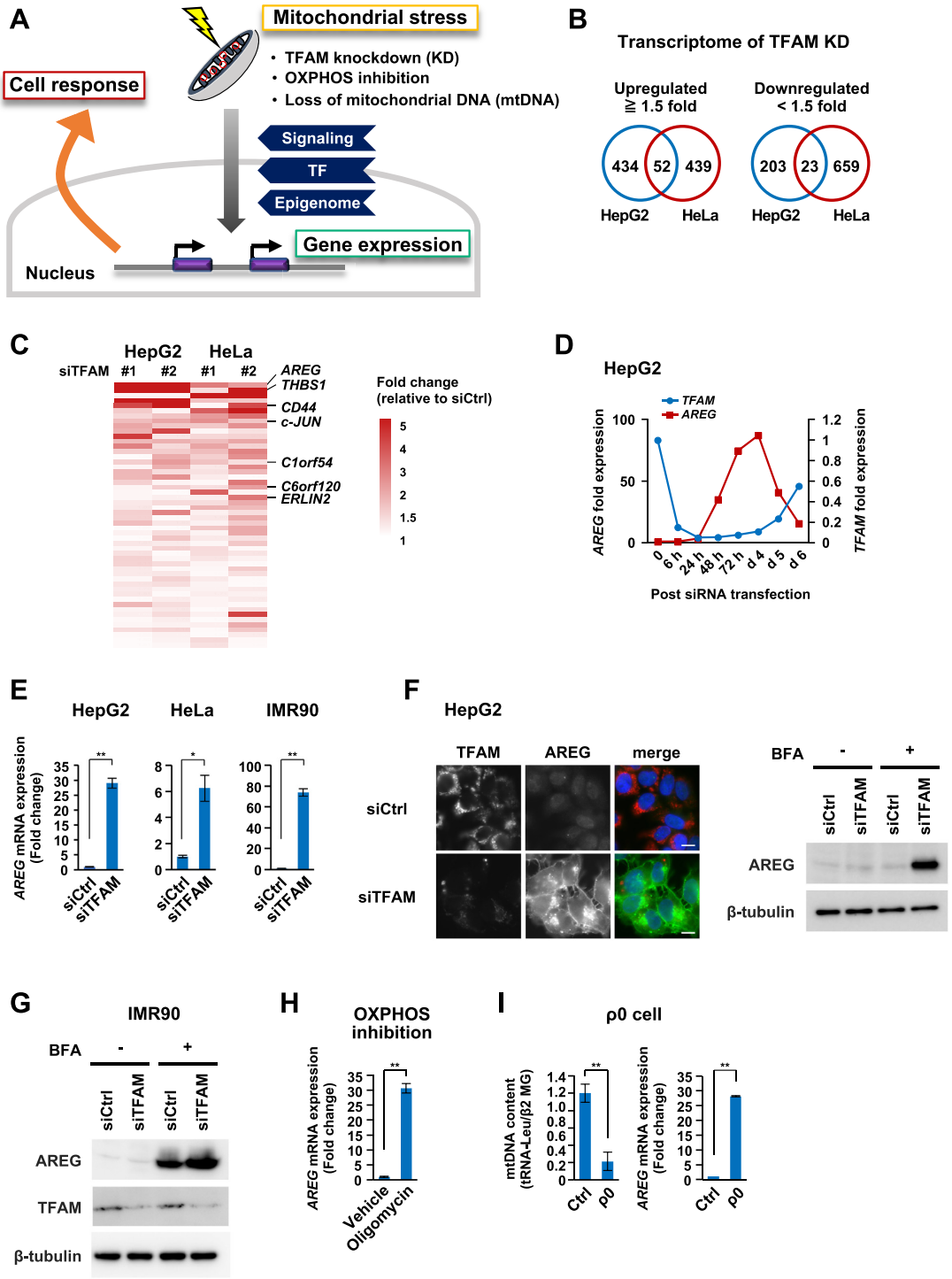

Figure 1. Transcriptome analyses identify AREG as a mitochondrial stress-induced secretory factor. (**A**) Study of mitochondrial stress-induced cellular response. Mitochondrial stresses stimulate signaling, transcriptional and epigenomic changes for nuclear gene control. (**B**) Transcriptome analyses of TFAM knockdown (KD) cells. The Venn diagrams show the number of genes whose expression levels changed by ≥1.5-fold after the distinct TFAM-KD experiments (siTFAM #1 or #2) in HepG2 and HeLa cells. (**C**) The top-ranked genes commonly upregulated by TFAM-KD include *AREG* and *THBS1* (Supplementary Table S3). Among them, secretory protein genes are shown in the heatmap. (**D**) Inverse correlation of *TFAM* and *AREG* mRNAs after TFAM-KD. RT-qPCR analysis was conducted in the time course. siTFAM #1 was indicated as 'siTFAM' in most experiments throughout the study. (**E**) Induction of *AREG* mRNA by TFAM-KD. TFAM-KD for 72 h in HepG2, HeLa cells and IMR90 fibroblasts. mRNA levels were normalized by the *RPLP0* (ribosomal protein lateral stalk subunit P0) gene and were indicated by mean ± SD ($n = 3$). $^{**}P < 0.01$, $^{*}P < 0.05$. (**F**) Immunofluorescence and western blot analyses of AREG protein in HepG2 cells. TFAM-KD was carried out for 72 h (left); scale bar: 10 μm. The cells were then treated with 5 μg/ml of brefeldin A (BFA) for 6 h to store intracellular AREG without being secreted (right). (**G**) Accumulation of AREG in IMR90 cells by TFAM-KD and BFA treatment. (**H,I**) Induction of *AREG* mRNA by various mitochondrial stresses. HepG2 treated with 0.5 μg/ml oligomycin for 24 h (H), HepG2-derived ρ0 cells established by ethidium bromide treatment for 10 days (I). mRNA levels were analyzed as described in panel (E).

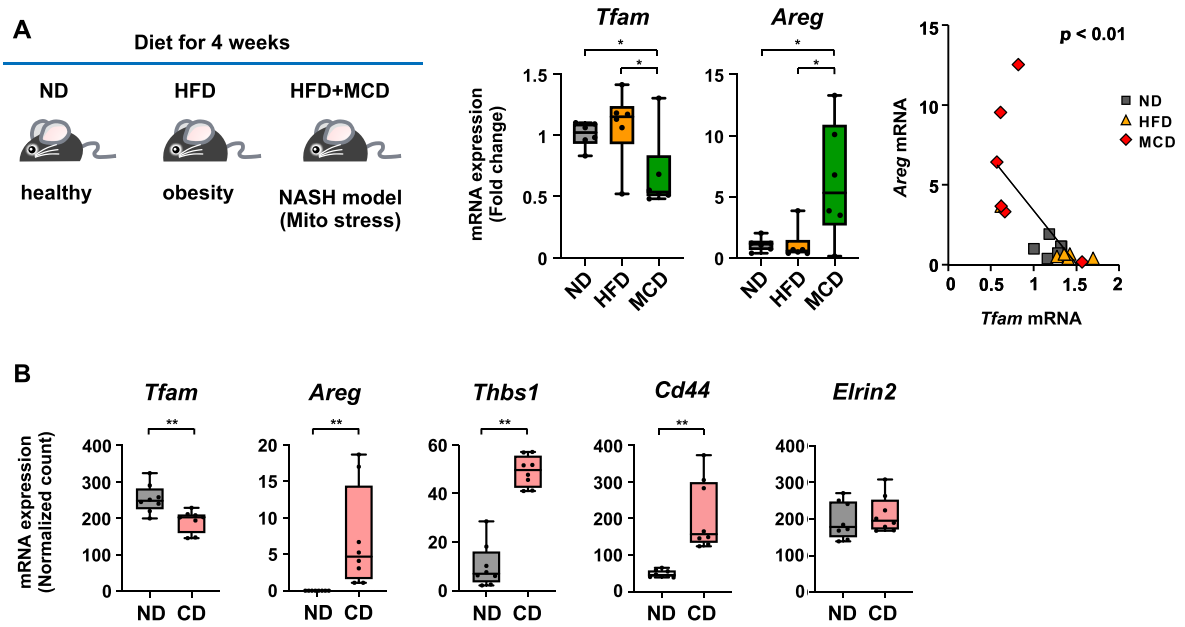

Figure 2. *Tfam* downregulation and *Areg* upregulation in mouse liver tissues under mitochondrial stresses *in vivo*. (**A**) Diet-induced murine NASH model corresponding to mitochondrial stresses. Seven-week-old male C57BL/6J mice were fed with normal diet (ND), high-fat diet (HFD) and HFD in combination with methionine and choline deficiency (MCD) for 4 weeks. RT-qPCR analysis of *Tfam* and *Areg* mRNAs from liver sections ($n = 6$). Box plot data are shown by the median and minimum/maximum whiskers. Inverse correlation between *Tfam* and *Areg* expression in the MCD group (right). Pearson product-moment correlation coefficient and *P* values are indicated. (**B**) Expression of mitochondrial stress-related genes such as *Tfam*, *Areg*, *Thbs1* and *Cd44* in L-amino acid-defined HFD/choline deficiency (CD)-fed mice that had moderate liver injury ($n = 8$). Data are from GSE137449; $^{*}P < 0.05$, $^{**}P < 0.01$.

RE sites. We found constitutively accessible chromatin structure at RE1, RE2 and RE3 in both the control and TFAM-KD cells (Supplementary Figure S3B). Using the chromatin interaction database (ChromoContact) (40), we found that RE3 interacted with the promoter region of the 5′-located *AREG* gene, which formed an approximately 285 kb chromatin loop harboring two *AREG* genes in AREG-positive cells but not in AREG-negative cells (Supplementary Figure S3C). To directly assess the enhancer activity, functional reporter assays were conducted in which the human *AREG* promoter was fused to the *luciferase* reporter gene with various combinations of the RE sequences (Figure 3C). As expected, *AREG*/*luciferase* activities were induced by each RE and were synergistically augmented by combinations of RE under the TFAM-KD condition, suggesting that RE enhancers cooperatively regulate *AREG* induction.

To identify transcriptional regulators that directly target these *AREG* enhancers, we compared our ChIP-seq data with published datasets using ChIP-Atlas (http://chip-atlas.org/) (25). The RE sites showed high enrichment of c-JUN, c-FOS, YAP1 and TEAD proteins in various *AREG*-expressing cells (Figure 3D and Supplementary Table S4). In addition, BRG1/SMARCA4, p300 and MLL4/KMT2D were significantly co-localized in the RE enhancers.

We then examined the contribution of these RE-associated factors to AREG induction by TFAM depletion. Under TFAM-KD, the inhibition of c-JUN, YAP1 or TEAD1 resulted in the reduction of AREG at both the RNA and protein levels (Figure 3E and Supplementary Figure S3D), indicating that these transcription factors promoted AREG induction. In contrast, the loss of BRG1 upregulated AREG expression (Figure 3F and Supplementary Figure S3D,E), indicating that this ATP-dependent chromatin remodeler suppressed AREG expression. Since BRG1 was decreased under TFAM-KD (Supplementary Figure S3F), in parallel with a decline in intracellular ATP (Supplementary Figure S1C), BRG1 activity might have been suppressed by mitochondrial dysfunction. Collectively, these results indicate that AREG expression is induced by dynamic activities of positive and negative regulators under mitochondrial stress.

c-JUN is upregulated by mitochondrial stress and directly promotes *AREG* expression

We next sought to gain mechanistic insights into how mitochondrial stress-responsive *AREG* enhancers are regulated. Among the factors involved in the upregulation of *AREG* genes, we first focused on c-JUN, since *c-JUN* expression was dramatically induced under TFAM-KD (Figure 1C), and all three RE enhancers contains the consensus motif for AP1 complex (c-FOS/c-JUN) (Supplementary Table S5). We found that phosphorylated c-JUN (p-c-JUN) at Ser73, a functionally active form of this protein (35,48–50), was increased in the nuclear fraction of the TFAM-KD cells (Figure 4A). Phosphorylated c-JUN was also increased in TFAM-depleted HeLa or IMR90 cells and in oligomycin-treated HepG2 cells (Supplementary Figure S4A). Consistently, p-c-JUN abundantly bound to the RE enhancers under TFAM inhibition, indicating its dynamic participation in the mitochondrial stress response (Figure 4B). To fur-

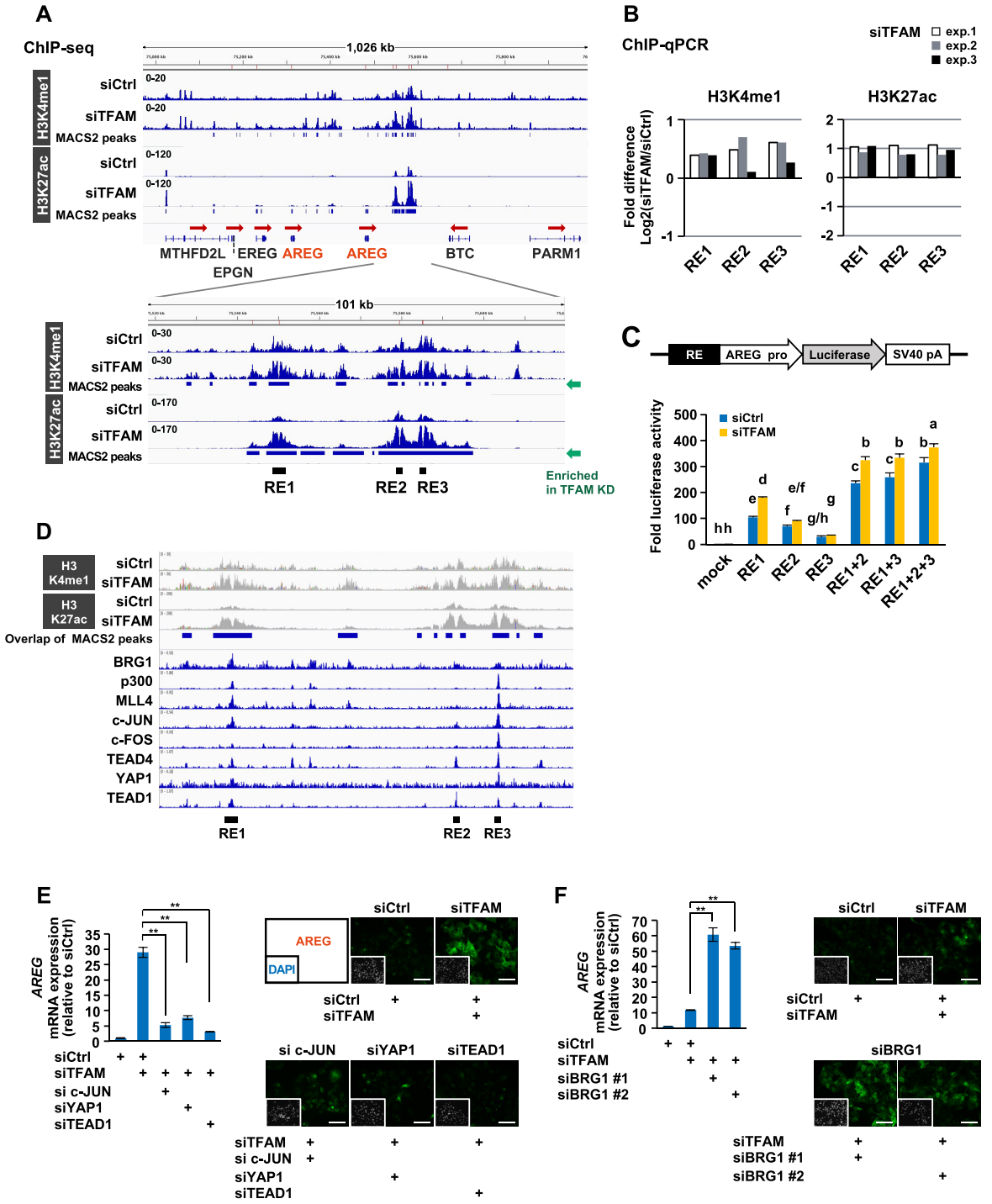

Figure 3. Epigenomic analyses reveal multiple transcriptional regulators acting on *AREG* gene enhancers under mitochondrial stress. (**A**) ChIP-seq analyses of active enhancer marks (H3K4me1 and H3K27ac) in HepG2 cells. After TFAM-KD for 72 h, enhancer marks-enriched sites were found between *AREG* and *betacellulin* (*BTC*) genes, named as RE1, RE2 and RE3. (**B**) Verification of H3K4me1 and H3K27ac enrichments at RE sites. Three independent ChIP-qPCR analyses were conducted under conditions similar to those in (**A**). The bars indicate the relative changes of modified histones (TFAM-KD versus control-KD) on a log2 scale. (**C**) Enhancer activity assay of single or multiple combinations of RE fused to *AREG* promoter-driven *luciferase* gene. Control and TFAM-KD HepG2 cells were analyzed 48 h after reporter plasmid transfection ($n = 3$). Differences in letters above the bars (a-h) indicate significant differences (Tukey's HSD test, $P < 0.05$). (**D**) ChIP-Atlas analysis of transcriptional regulators at mitochondrial stress-responsive RE enhancers. The datasets were extracted from the top-ranked fold enrichment (Supplementary Table S4). The ChIP-seq data are from GSM1835989 for BRG1, GSM1240110 for p300, GSM1240109 for MLL4, GSM1700784 for c-JUN, GSM777644 for c-FOS, GSM1010772 for TEAD4, GSM1614029 for YAP1 and GSM1667161 for TEAD1. (**E, F**) Knockdown effects of RE-associated transcriptional regulators on AREG induction by TFAM depletion. RT-qPCR and immunofluorescence analyses were performed using indicated combinations of siRNAs against TFAM and each factor for 72 h in HepG2 cells; scale bar: 100 μm; $^{**}P < 0.01$.

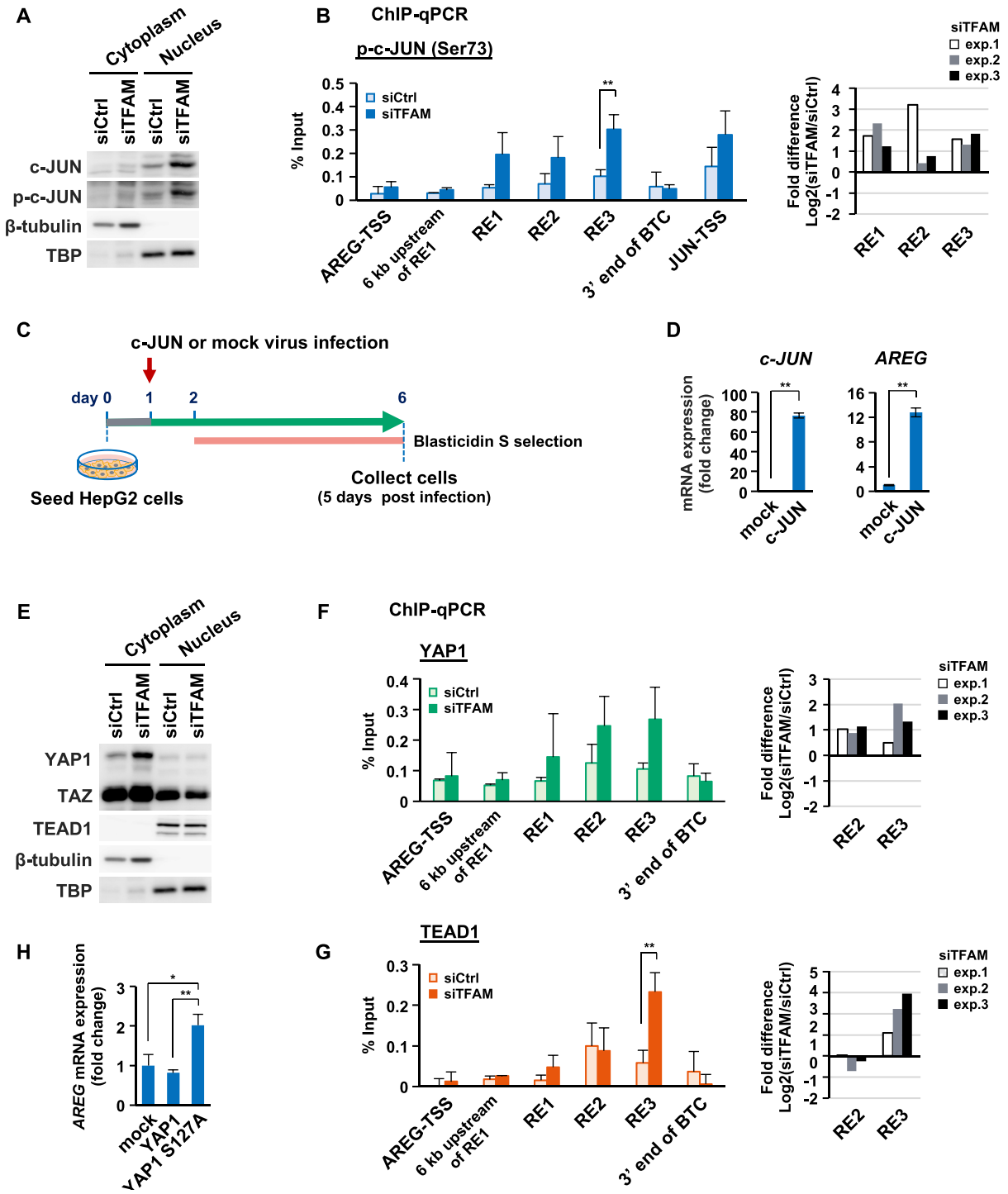

Figure 4. c-JUN and activated YAP1/TEAD1 induce *AREG* expression under mitochondrial stress. (**A**) Western blot analysis of c-JUN and p-c-JUN (phosphorylated c-JUN at Ser73) in cytoplasmic and nuclear fractions from HepG2 cells (control and TFAM-KD for 72 h). (**B**) ChIP-qPCR analysis of p-c-JUN at RE sites in the *AREG* gene region. Control and TFAM-KD cells for 72 h were tested ($n = 3$). Transcription start sites (TSSs) of *AREG* and *JUN* genes were used as negative and positive controls, respectively (left). Data are represented as mean ± SD. ** $P < 0.01$. Based on Supplementary Table S5, fold difference bars indicate the relative enrichments of p-c-JUN for the three REs (TFAM-KD vs. control-KD) on a log2 scale (right). (**C**) Overexpression of c-JUN using lentivirus gene transfer and blasticidin S selection in HepG2 cells. Representative images of mock and c-JUN-expressing virus infected cells (day 7) (Supplementary Figure S4B). (**D**) Expression of *c-JUN* and *AREG* in c-JUN overexpressing cells ($n = 3$); ** $P < 0.01$, * $P < 0.05$. (**E**) Western blot analysis of YAP1, TAZ, and TEAD1 in cytoplasmic and nuclear fractions from HepG2 cells (control and TFAM-KD for 72 h). (**F, G**) ChIP-qPCR analysis of YAP1 (F) and TEAD1 (G) at RE sites in the *AREG* gene region. Control and TFAM-KD cells for 72 h were tested ($n = 3$). TSS of *AREG* gene and other sites were used as negative controls (left). Data are represented as mean ± SD. **$P < 0.01$. Based on Supplementary Table S5, fold difference bars indicate the relative enrichments of YAP1 and TEAD1 at RE2/3 enhancers (TFAM-KD versus control-KD) on a log2 scale (right). (**H**) RT-qPCR analysis of *AReG* mRNA; $n = 3$, **$P < 0.01$, *$P < 0.05$.

ther test the involvement of c-JUN in *AREG* expression, we introduced a lentiviral vector to force c-JUN expression (Figure 4C). Interestingly, c-JUN overexpression strongly induced *AREG* expression (Figure 4D). Under these conditions, we observed no evident cell damage (Supplementary Figure S4B), or no changes in the expression of *TFAM* and mtDNA-coded genes such as cytochrome c oxidase subunit 1 (*CO1*), NADH dehydrogenase 1 (*ND1*) and NADH dehydrogenase 6 (*ND6*), or in the relative copy numbers of mtDNAs (Supplementary Figure S4C). Interestingly, the use of the JNK inhibitor, SP600125, did not significantly inhibit c-JUN phosphorylation and *AREG* induction under the TFAM-KD (Supplementary Figure S4D) (see the Discussion). These results suggest that mitochondrial dysfunction upregulates c-JUN, which in turn strongly enhance *AREG* expression.

Activated YAP1 targets *AREG* gene enhancers

We then examined the involvement of YAP1 and TEAD1 in the mitochondrial stress response, since *YAP1* expression was upregulated in parallel with *AREG* and *c-JUN* in TFAM-KD HepG2 cells (Supplementary Figure S4E). YAP1 is phosphorylated and stabilized by the LAT kinases, whereas dephosphorylated YAP1 translocates to the nucleus, regulates gene expression together with TEAD1, and is then degraded by the proteasome pathway (51). TFAM depletion evidently increased cytoplasmic YAP1 in HepG2 cells (Figure 4E), but nuclear YAP1 was undetectable probably due to its degradation. The amount of TEAD1 in the nuclei was not affected by TFAM-KD. Similarly, TFAM depletion increased the total YAP1 as well as phosphorylated c-JUN in HeLa and IMR90 cells (Supplementary Figure S4A). The RE2/3 enhancers of the *AREG* genes, which contains the TEAD-binding motifs (Supplementary Table S5), were targeted by YAP1 and TEAD1 under TFAM-KD, indicating that YAP1 was actively involved in *AREG* induction (Figure 4F,G). To validate this event, we used lentivirus gene transfer to examine the overexpressing effect of wild-type YAP1 and constitutively active YAP1 (S127A; phosphorylation-defective) on *AREG* expression (Supplementary Figure S5A). Overexpression of YAP1 caused no evident cell damage. FLAG-tagged YAP1 (S127A) was short-lived at the protein level and was predominantly localized to the nucleus (Supplementary Figure S5B). Interestingly, YAP1 (S127A) overexpression moderately increased *AREG* expression (Figure 4H and Supplementary Figure S5B), possibly via the enrichment of YAP1 (S127A) and TEAD1 at RE2 (Supplementary Figure S5C), suggesting that YAP1 functions for AREG induction.

c-JUN and YAP1 cooperatively upregulate *AREG* and *THBS1* genes

To investigate the cooperative role of c-JUN and YAP1, we examined the effect of co-expression of c-JUN with either YAP1 or YAP1 (S127A) in HepG2 cells (Figure 5A). We did not observe any mutual influence on the expression levels. Co-expression of c-JUN and YAP1 (S127A) upregulated the expression of *AREG* (Figure 5B), with an amplitude similar to TFAM-KD (Figure 1E). Notably, the combination of c-JUN and YAP1 did not affect the expression of *TFAM*, and mtDNA-coded *CO1*, *ND1* and *ND6* genes, suggesting that c-JUN and YAP1 enhanced the expression of AREG without inducing mitochondrial dysfunction.

In addition to AREG, we found a number of secretory protein-encoding genes, whose expression was significantly upregulated by TFAM-KD (Figure 1C). Among them, *THBS1* was also upregulated by the co-expression c-JUN and YAP1 (Figure 5B). Our ChIP-seq analyses revealed that TFAM-KD increased the levels of both H3K4me1 and H3K27ac at the proximal and upstream distal enhancers of *THBS1*, which were occupied by c-JUN and YAP1/TEAD1 (Figure 5C). Similar data were obtained in genes encoding other secretory proteins, including *CD44*, *C1orf54* (hypothetical) and *ERLIN2* (Supplementary Figure S6), indicating that c-JUN and YAP1 play central roles in shaping mitochondrial stress-associated transcriptome. Further, this finding was emphasized by our data that AREG, THBS1, p-c-JUN and YAP1 were upregulated in ρ0 cells, while TFAM clearly disappeared (Supplementary Figure S7).

The loss of TFAM triggers epigenetic remodeling at enhancers associated with stress response and metabolism pathways

To explore whether c-JUN/YAP1/TEAD1 axis is prevalent in the chromatin regulation under mitochondrial stress, we analyzed the enrichment of transcription factor-binding motifs in regions with altered enhancer marks (H3K4me1 and H3K27ac) by TFAM-KD. JUN/AP-1 and TEAD consensus sequences were listed at the top-ranked motifs in regions with increased active enhancer marks (Figure 6A). Consistently, under TFAM-KD, enhancer marks were accumulated near the c-JUN- or YAP1-bound sites which were defined using publicly available ChIP-seq data (Figure 6B). By a functional enrichment analysis using clusterProfiler, we found that genes associated with various stress response pathways were enriched in 309 genes which were bound by c-JUN and upregulated by TFAM-KD with enriched enhancer marks (Figure 6C,D and Supplementary Table S6). In addition, both similar and unique pathways were enriched in 195 genes which were bound by YAP1 and upregulated by TFAM-KD with enriched enhancer marks (Figure 6D,E and Supplementary Table S6). Actually, 175 of the 195 YAP1-targeted genes were merged with the c-JUN-targeted genes (Supplementary Figure S8A). These results indicate that TFAM depletion triggers a c-JUN- and YAP-mediated epigenetic remodeling leading to stress responses. Notably, gene concept-network (cnet) plot analyses showed that these c-JUN- and YAP1-targeted genes encoded many secretory proteins such as AREG and THBS1 (Supplementary Figure S8B,C).

On the other hand, we found enriched binding motifs for cell type-specific transcription factors such as hepatocyte nuclear factor-4α (HNF4α) in regions with reduced enhancer marks by TFAM-KD (Figure 6A). Consistently, HNF4α-bound enhancers showed decreased H3K27ac levels in the TFAM-KD HepG2 cells (Figure 6B). 325 HNF4α-bound genes were overlapped with transcriptional downregulation and decreased enhancer marks under TFAM-KD (Figure 6F and Supplementary Table S6).

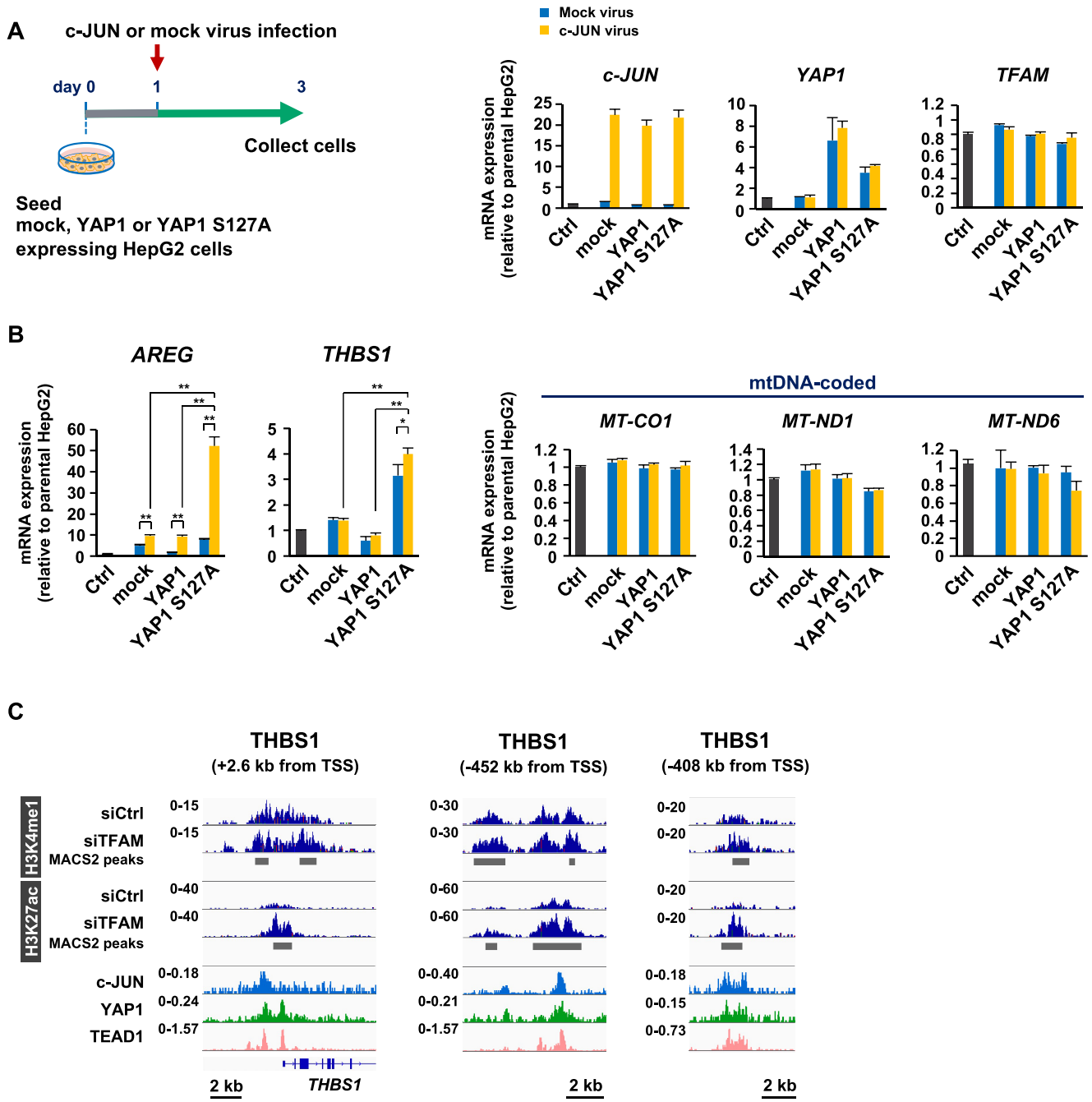

Figure 5. (**A**) Preparation of HepG2 cells that co-overexpressed c-JUN and YAP1 by lentivirus gene transfer. Expression levels of *c-JUN*, *YAP1* and *YAP1(S127A)* mRNAs. (**B**) RT-qPCR analysis of *AREG* and *THBS1*, and mitochondria-related genes. $n = 3$, data are represented as mean ± SD; $^{**}P < 0.01$, $^{*}P < 0.05$. (**C**) Coexistence of active marks (H3K4me1 and H3K27ac), c-JUN and YAP1/TEAD1 in the proximal and distal enhancers of *THBS1* gene. ChIP-seq data are from GSM1700784 for c-JUN, GSM1614029 for YAP1 and GSM1667161 for TEAD1.

Functional enrichment analysis of 325 overlapping genes revealed the pathways involved in liver-specific metabolic processes (Figure 6G), suggesting that multiple metabolic genes were influenced by HNF4α under mitochondrial stress. A large portion of such genes were positively regulated by HNF4α under normal condition (Supplementary Figure S8D), suggesting that HNF4α function may be compromised under mitochondrial dysfunction. Taken together, our study highlighted that TFAM depletion triggers a unique retrograde signaling to transcriptional and epigenetic reprogramming, possibly resulting in a shift from metabolism to stress responses including protein secretion.

DISCUSSION

Mitochondria-to-nucleus signaling profoundly contributes to cellular functions and homeostasis. Although key players for such retrograde signaling including metabolites, ki-

A

Enriched motifs in regions with increased active enhancer mark by TFAM KD (5184 regions)

	p-value	Targets	Background
JUN (AP-1)	1e-549	43.94%	14.82%
ERG (ETS)	1e-78	24.19%	14.32%
Chop, ATF4	1e-34	1.74%	0.33%
HSF4, TEAD	1e-33	0.95%	0.08%

Enriched motifs in regions with reduced active enhancer mark by TFAM KD (3805 regions)

	p-value	Targets	Background
HNF4α	1e-121	14.32%	4.51%
RAR:RXR	1e-66	8.64%	2.87%
HNF1β	1e-35	12.37%	6.73%

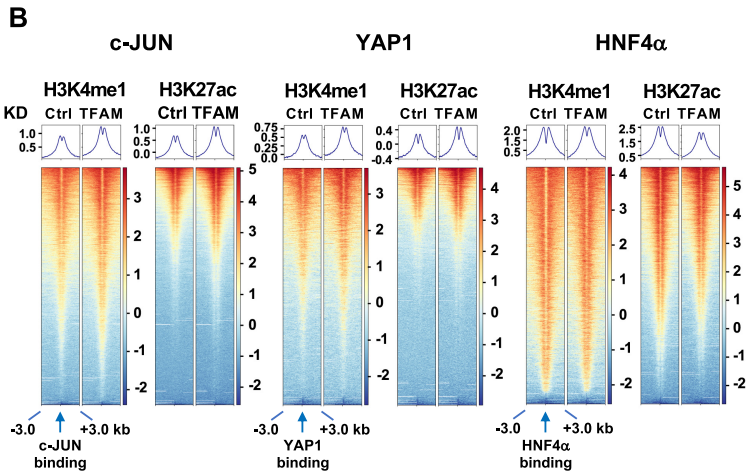

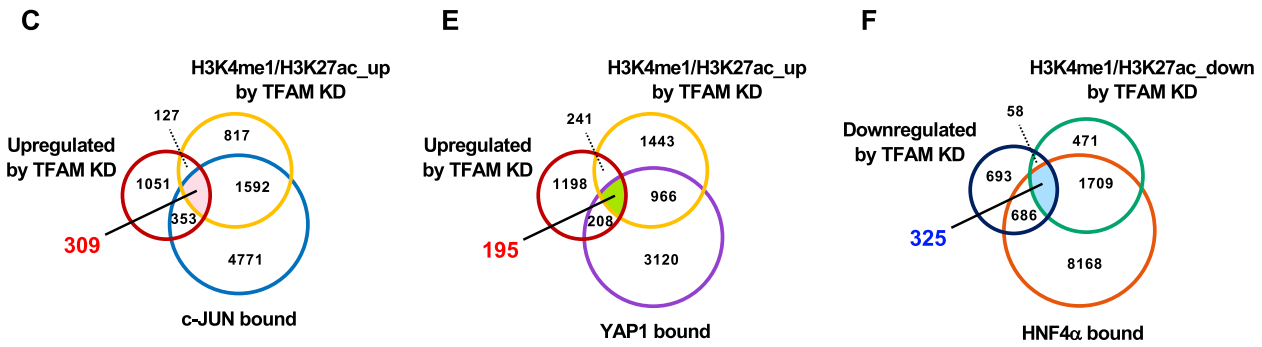

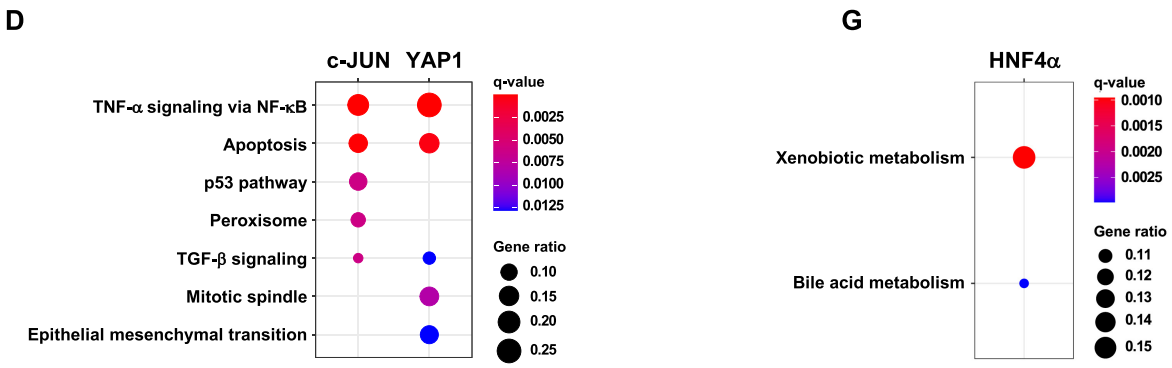

Figure 6. Genome-wide gene regulation mediated by c-JUN, YAP1 and HNF4α under mitochondrial stress. (**A**) Enriched motifs in the regions with increased or decreased enhancer marks (H3K4me1 and H3K27ac) in TFAM depleted-HepG2 cells. Motifs for transcription factor binding were identified using the HOMER algorithm. (**B**) Enhancer marks near c-JUN, YAP1 or HNF4α binding sites (–3 to + 3 kb) in control and TFAM-KD cells. Normalized enrichment values are from GSM1700784 for c-JUN, GSM1614029 for YAP1 and GSM469863 for HNF4α. (**C,E**) Venn diagram of 309 genes merged with transcriptional upregulation (≥1.5-fold in TFAM-KD), increased enhancer marks by TFAM-KD and c-JUN binding (C), and 195 genes merged with transcriptional upregulation (≥1.5-fold in TFAM-KD), increased enhancer marks by TFAM-KD and YAP1 binding (E) (listed in Supplementary Table S6). (**D**) Top five Molecular Signatures Database (MSigDB) Hallmark pathways enriched in 309 c-JUN target genes (C) and 195 YAP1 target genes (E). The gene ratios of Peroxisome and TGF-β signaling in c-JUN targets and TGF-β signaling in YAP1 targets were 0.08, 0.05 and 0.06, respectively. FDR < 0.05. (**F**) Venn diagram of 325 genes merged with transcriptional downregulation (≥1.5-fold in TFAM-KD), decreased enhancer marks by TFAM-KD, and HNF4α binding (listed in Supplementary Table S6). (**G**) The MSigDB Hallmark pathways enriched in 325 overlapped genes (F). The gene ratios for Xenobiotic metabolism and Bile acid metabolism were 0.16 and 0.10, respectively; FDR < 0.05.

nases and transcriptional regulators have been identified, not much is known about how these players dynamically communicate to generate specific gene expression patterns. Here, we found that the loss of TFAM caused mitochondrial dysfunction, stimulated cooperation of c-JUN and YAP1, and induced expression of the *AREG* gene with transcriptionally active marks at newly identified RE enhancers. Further, investigations of murine NAFLD/NASH models showed that *Areg* gene was upregulated, while the *Tfam* gene was downregulated in the liver tissues, suggesting that AREG expression is a hallmark of mitochondrial dysfunction in the liver. Thus, multiple signaling pathways cooperate to specifically induce transcriptional and epigenetic alterations when mitochondria are damaged.

Communication between the nucleus and mitochondria consists of anterograde and retrograde pathways (1). TFAM is a well-known transcription factor acting on mtDNA in the anterograde pathway (3,6,52). We found that TFAM depletion directly initiated mitochondrial stress or dysfunction, followed by a subsequent retrograde pathway. Thus, these bidirectional pathways are continuously linked to each other as a biological cycle. We also found that mitochondrial stress is transmitted to the nucleus via activation of c-JUN and YAP-mediated signaling, and that the resulting cells reprogram gene expression, allowing unique protein production and secretion. Although c-JUN is known to be functionally activated via its phosphorylation by the JNK (35,48–50), we observed that the JNK inhibitor, SP600125, did not diminish the increase in phosphorylated c-JUN under the TFAM-KD (Supplementary Figure S4D), indicating that other kinases may operate for this mitochondrial stress response. In addition, YAP proteins translocate to the nucleus through dephosphorylation mediated by protein phosphatase 2A (PP2A) (51,53). The use of the PP2A inhibitor, LB-100, increased the phosphorylated form of YAP1 under TFAM-KD (data not shown), suggesting that PP2A is involved in the mitochondrial stress response. However, our experimental condition using TFAM-KD may represent the early stage of mitochondrial dysfunction, as gene sets involved in the mitochondrial unfolded protein response (UPRmt) (54,55) did not vary in the cells tested (data not shown). If c-JUN and YAP1 are more essential for acute response to mitochondrial stress, it may be reasonable that we observed no evident upregulation of *c-Jun* and *Yap1* mRNAs in murine NAFLD/NASH models (data not shown). In addition, the loss of *Tfam* might have distinct effects on gene control including *Areg* expression, depending on cell types and experimental conditions (56).

Our ChIP-seq investigations revealed that mitochondrial stress frequently activated distal enhancers of target genes, which were enriched with c-JUN and YAP1/TEAD1 binding (Figures 3D, 5C and Supplementary Figure S6). Additionally, such distal enhancers were accompanied by the accumulation of chromatin remodeling factors such as p300, MLL4, and BRG1 in the *AREG* gene (Figure 3D and data not shown in other genes). It has been previously reported that AP-1 (c-FOS/c-JUN) and YAP/TAZ/TEAD are colocalized at distal enhancers of proliferative genes and promote growth via chromatin loop formation between enhancers and promoters in breast cancer cells (27). In fibroblasts, the AP-1 complex, together with TEAD and lineage-specific transcription factors, binds to nucleosome-occluded enhancers and recruits the BAF chromatin remodeling complex to establish an accessible chromatin state (57). These results suggest that c-JUN and YAP/TEAD collaborate with the chromatin remodeling complex at distal enhancers to induce selective expression of target genes. In other words, combinations of c-JUN and YAP/TEAD may be an enhancer repertoire strategy.

For the YAP-driven cell growth and tumorigenesis, robust YAP binding was restricted to a relatively small number of hyperactive distal enhancers. YAP interacted with the transcriptional mediator complexes at the enhancers, which allowed the recruitment of cyclin-dependent kinase 9, which regulated the promoter-proximal polymerase II (Pol II) pause release (58). This enabled rapid and regulatory gene induction, similar to the immediate early genes (59,60). Consistently, we found that the mediator complex subunit 1 (MED1) and cyclin-dependent kinase 8 accumulated at the YAP1-enriched RE enhancers of the *AREG* gene (data not shown). Thus, acute mitochondrial stress responses may utilize the Pol II pause release to support rapid gene control.

Interestingly, mitochondrial stress induced production or secretion of newly synthesized proteins such as AREG and THBS1. AREG is an autocrine or paracrine growth modulatory factor while THBS1 plays a role in extracellular matrix and cell-to-cell interactions. Both proteins have been demonstrated to control the proliferation of various cells under developmental, inflammatory, senescent and cancerous conditions (61–63). There is the possibility that this secretion is a compensatory growth-promoting alert from mitochondrial dysfunction cells to acceptor cells in the tissue.

Cellular senescence is induced by various stresses, such as oncogene induction, telomere attrition, DNA damage, and deregulation of chromatin. Senescent cells have been found to cause mitochondrial dysfunction, either activation or decline, and a proinflammatory program referred to as the senescence-associated secretory phenotype (SASP) (64,65). Wiley *et al*. have reported that knockdown of sirtuin 3 (SIRT3), a mitochondrial sirtuin, led to senescence in human fibroblasts which was not accompanied by the expression of proinflammatory cytokines (66). Interestingly, SIRT3 depletion-induced senescent cells upregulated the *AREG* and *IL-10* genes. This may be consistent with our results that cells undergoing mitochondrial dysfunction acquired the unique production of AREG and THBS1 in hepatic cells and liver tissues.

Chronic liver diseases such as NAFLD/NASH represent hepatic triglyceride accumulation, mitochondrial dysfunction, and cellular senescence in the liver (15–18). Mitochondrial stress is deeply implicated in the development of these diseases, as the activities of OXPHOS and ATP synthesis decrease in liver tissues from these patients. Importantly, hepatic lipid overload is known to induce a c-JUN-mediated stress response, which is often associated with NAFLD pathogenesis (35). In the present study, murine NAFLD/NASH models showed upregulation of *Areg* and downregulation of *Tfam* gene in liver tissues (Figure 2). The human liver transcriptome of NAFLD patients exhibited a similar tendency of *AREG* and *TFAM* expression (Supplementary Figure S2). Our data suggest that alteration of anterograde and/or retrograde pathways contributes to

NAFLD/NASH pathophysiology, which may be emerging diagnostic/therapeutic targets.

Taken together, our study highlights the molecular basis of mitochondria-to-nucleus signaling and the mitochondrial stress-induced transcriptional and epigenomic remodeling, and promotes our understanding of the mitochondrial dysfunction-driven cellular responses.

DATA AVAILABILITY

The sequencing data generated for this study are available in the Gene Expression Omnibus (GEO) database (GSE196511 and GSE197242).

SUPPLEMENTARY DATA

Supplementary Data are available at NAR Online.

ACKNOWLEDGEMENTS

We thank the members in our laboratory for helpful discussions, especially Dr. Tatsuro Yamamoto for assisting data analyses.

FUNDING

JSPS KAKENHI [21H02686, 20KK0185 to M.N., 20H04108, 21K19513 to S.H.]; Takeda Science Foundation (to M.N., S.H.); Naito Foundation (to M.N.); Japan Agency for Medical Research and Development [21gk0210029h0101 to S.H.]; the program of the Inter-University Research Network for High Depth Omics, IMEG, Kumamoto University. Funding for open access charge: JSPS KAKENHI.

Conflict of interest statement. None declared.

REFERENCES

1. Quirós,P.M., Mottis,A. and Auwerx,J. (2016) Mitonuclear communication in homeostasis and stress. *Nat. Rev. Mol. Cell Biol.*, **17**, 213–226.
2. Mottis,A., Herzig,S. and Auwerx,J. (2019) Mitocellular communication: shaping health and disease. *Science*, **366**, 827–832.
3. Weinhouse,C. (2017) Mitochondrial-epigenetic crosstalk in environmental toxicology. *Toxicol.*, **391**, 5–17.
4. Larsson,N.-G., Wang,J., Wilhelmsson,H., Oldfors,A., Rustin,P., Lewandoski,M., Barsh,G.S. and Clayton,D.A. (1998) Mitochondrial transcription factor a is necessary for mtDNA maintance and embryogenesis in mice. *Nat. Genet.*, **18**, 231–236.
5. Parisi,M.A. and Clayton,D.A. (1991) Similarity of human mitochondrial transcription factor 1 to high mobility group proteins. *Science*, **252**, 965–969.
6. Scarpulla,R.C. (2008) Transcriptional paradigms in mammalian mitochondrial biogenesis and function. *Physiol. Rev.*, **88**, 611–638.
7. Anan,K., Hino,S., Shimizu,N., Sakamoto,A., Nagaoka,K., Takase,R., Kohrogi,K., Araki,H., Hino,Y., Usuki,S. *et al.* (2018) LSD1 mediates metabolic reprogramming by glucocorticoids during myogenic differentiation. *Nucleic Acids Res.*, **46**, 5441–5454.
8. Hino,S., Sakamoto,A., Nagaoka,K., Anan,K., Wang,Y., Mimasu,S., Umehara,T., Yokoyama,S., Kosai,K.I. and Nakao,M. (2012) FAD-dependent lysine-specific demethylase-1 regulates cellular energy expenditure. *Nat. Commun.*, **3**, 758.
9. Tanaka,H., Takebayashi,S., Sakamoto,A., Igata,T., Nakatsu,Y., Saitoh,N., Hino,S. and Nakao,M. (2017) The SETD8/PR-Set7 methyltransferase functions as a barrier to prevent senescence-associated metabolic remodeling. *Cell Rep.*, **18**, 2148–2161.
10. Nakao,M., Anan,K., Araki,H. and Hino,S. (2019) Distinct roles of the NAD+-Sirt1 and FAD-LSD1 pathways in metabolic response and tissue development. *Trends Endocrinol. Metab.*, **30**, 409–412.
11. Nakao,M., Tanaka,H. and Koga,T. (2020) Cellular senescence variation by metabolic and epigenomic remodeling. *Trends Cell Biol.*, **30**, 919–922.
12. Scher,M.B., Vaquero,A. and Reinberg,D. (2007) SirT3 is a nuclear NAD^+-dependent histone deacetylase that translocates to the mitochondria upon cellular stress. *Genes Dev.*, **21**, 920–928.
13. Schwer,B., North,B.J., Frye,R.A., Ott,M. and Verdin,E. (2002) The human silent information regulator (Sir)2 homologue hSIRT3 is a mitochondrial nicotinamide adenine dinucleotide–dependent deacetylase. *J. Cell Biol.*, **158**, 647–657.
14. Cardamone,M.D., Tanasa,B., Cederquist,C.T., Huang,J., Mahdaviani,K., Li,W., Rosenfeld,M.G., Liesa,M. and Perissi,V. (2018) Mitochondrial retrograde signaling in mammals is mediated by the transcriptional cofactor GPS2 via direct mitochondria-to-nucleus translocation. *Mol. Cell*, **69**, 757–772.
15. Loomba,R., Friedman,S.L. and Shulman,G.I. (2021) Mechanisms and disease consequences of nonalcoholic fatty liver disease. *Cell*, **184**, 2537–2564.
16. Mansouri,A., Gattolliat,C.H. and Asselah,T. (2018) Mitochondrial dysfunction and signaling in chronic liver diseases. *Gastroenterol.*, **155**, 629–647.
17. Samuel,V.T. and Shulman,G.I. (2018) Nonalcoholic fatty liver disease as a nexus of metabolic and hepatic diseases. *Cell Metab.*, **27**, 22–41.
18. Sunny,N.E., Bril,F. and Cusi,K. (2017) Mitochondrial adaptation in nonalcoholic fatty liver disease: novel mechanisms and treatment strategies. *Trends Endocrinol. Metab.*, **28**, 250–260.
19. Nass,M.M. (1970) Abnormal DNA patterns in animal mitochondria: ethidium bromide-induced breakdown of closed circular DNA and conditions leading to oligomer accumulation. *Proc. Natl. Acad. Sci. USA*, **67**, 1926–1933.
20. Rooney,J., Ryde,I., Sanders,L., Howlett,E., Colton,M., Germ,K., Mayer,G., Greenamyre,J. and Meyer,J. (2015) PCR based determination of mitochondrial DNA copy number in multiple species. *Methods Mol Biol.*, **1241**, 23–38.
21. Bolotin,E., Liao,H., Ta,T.C., Yang,C., Hwang-Verslues,W., Evans,J.R., Jiang,T. and Sladek,F.M. (2010) Integrated approach for the identification of human hepatocyte nuclear factor 4α target genes using protein binding microarrays. *Hepatol.*, **51**, 642–653.
22. Saitoh,N., Sakamoto,C., Hagiwara,M., Agredano-Moreno,L.T., Jimeńez-Garciá,L.F. and Nakao,M. (2012) The distribution of phosphorylated SR proteins and alternative splicing are regulated by RANBP2. *Mol. Biol. Cell*, **23**, 1115–1128.
23. Li,H. and Durbin,R. (2009) Fast and accurate short read alignment with burrows-wheeler transform. *Bioinformatics*, **25**, 1754–1760.
24. Zhang,Y., Liu,T., Meyer,C.A., Eeckhoute,J., Johnson,D.S., Bernstein,B.E., Nussbaum,C., Myers,R.M., Brown,M., Li,W. *et al.* (2008) Model-based analysis of chip-Seq (MACS). *Genome Biol.*, **9**, R137.
25. Oki,S., Ohta,T., Shioi,G., Hatanaka,H. and Ogasawara,O. (2018) ChIP-Atlas: a data-mining suite powered by full integration of public chip-seq data. *EMBO Rep.*, **19**, e46255.
26. Chen,Z., Lan,X., Wu,D., Sunkel,B., Ye,Z., Huang,J., Liu,Z., Clinton,S.K., Jin,V.X. and Wang,Q. (2015) Ligand-dependent genomic function of glucocorticoid receptor in triple-negative breast cancer. *Nat. Commun.*, **6**, 8323.
27. Zanconato,F., Forcato,M., Battilana,G., Azzolin,L., Quaranta,E., Bodega,B., Rosato,A., Bicciato,S., Cordenonsi,M. and Piccolo,S. (2015) Genome-wide association between YAP/TAZ/TEAD and AP-1 at enhancers drives oncogenic growth. *Nat. Cell Biol.*, **17**, 1218–1227.
28. Daigo,K., Kawamura,T., Ohta,Y., Ohashi,R., Katayose,S., Tanaka,T., Aburatani,H., Naito,M., Kodama,T., Ihara,S. *et al.* (2011) Proteomic analysis of native hepatocyte nuclear factor-4α (HNF4α) isoforms, phosphorylation status, and interactive cofactors. *J. Biol. Chem.*, **286**, 674–686.
29. Heinz,S., Benner,C., Spann,N., Bertolino,E., Lin,Y.C., Laslo,P., Cheng,J.X., Murre,C., Singh,H. and Glass,C.K. (2010) Simple combinations of lineage-determining transcription factors prime

cis-regulatory elements required for macrophage and b cell identities. *Mol. Cell*, **38**, 576–589.
30. Ramírez,F., Ryan,D.P., Grüning,B., Bhardwaj,V., Kilpert,F., Richter,A.S., Heyne,S., Dündar,F. and Manke,T. (2016) deepTools2: a next generation web server for deep-sequencing data analysis. *Nucleic Acids Res.*, **44**, W160–W165.
31. Yu,G., Wang,L.G., Han,Y. and He,Q.Y. (2012) ClusterProfiler: an r package for comparing biological themes among gene clusters. *Omi. A J. Integr. Biol.*, **16**, 284–287.
32. Wu,T., Hu,E., Xu,S., Chen,M., Guo,P., Dai,Z., Feng,T., Zhou,L., Tang,W., Zhan,L. *et al.* (2021) clusterProfiler 4.0: a universal enrichment tool for interpreting omics data. *Innov.*, **2**, 100141.
33. Fishilevich,S., Nudel,R., Rappaport,N., Hadar,R., Plaschkes,I., Stein,T.I., Rosen,N., Kohn,A., Twik,M., Safran,M. *et al.* (2017) GeneHancer: Genome-wide integration of enhancers and target genes in genecards. *Database*, **2017**, bax028.
34. Robinson,J.T., Thorvaldsdóttir,H., Winckler,W., Guttman,M., Lander,E.S., Getz,G. and Mesirov,J.P. (2011) Integrative genomics viewer. *Nat. Biotechnol.*, **29**, 24–26.
35. Nagaoka,K., Hino,S., Sakamoto,A., Anan,K., Takase,R., Umehara,T., Yokoyama,S., Sasaki,Y. and Nakao,M. (2015) Lysine-specific demethylase 2 suppresses lipid influx and metabolism in hepatic cells. *Mol. Cell. Biol.*, **35**, 1068–1080.
36. Heintz,M.M., McRee,R., Kumar,R. and Baldwin,W.S. (2020) Gender differences in diet-induced steatotic disease in Cyp2b-null mice. *PLoS One*, **15**, e0229896.
37. Love,M.I., Huber,W. and Anders,S. (2014) Moderated estimation of fold change and dispersion for RNA-seq data with DESeq2. *Genome Biol.*, **15**, 550.
38. Waki,H., Nakamura,M., Yamauchi,T., Wakabayashi,K.ichi, Yu,J., Hirose-Yotsuya,L., Take,K., Sun,W., Iwabu,M., Okada-Iwabu,M. *et al.* (2011) Global mapping of cell type-specific open chromatin by FAIRE-seq reveals the regulatory role of the NFI family in adipocyte differentiation. *PLoS Genet.*, **7**, e1002311.
39. Whyte,W.A., Orlando,D.A., Hnisz,D., Abraham,B.J., Lin,C.Y., Kagey,M.H., Rahl,P.B., Lee,T.I. and Young,R.A. (2013) Master transcription factors and mediator establish super-enhancers at key cell identity genes. *Cell*, **153**, 307–319.
40. Sato,T. and Suyama,M. (2015) ChromContact: a web tool for analyzing spatial contact of chromosomes from Hi-C data. *BMC Genomics*, **16**, 1060.
41. Hou,J., Zhang,J., Cui,P., Zhou,Y., Liu,C., Wu,X., Ji,Y., Wang,S., Cheng,B., Ye,H. *et al.* (2021) TREM2 sustains macrophage-hepatocyte metabolic coordination in nonalcoholic fatty liver disease and sepsis. *J. Clin. Invest.*, **131**, e135197.
42. Quandt,K., Frech,K., Karas,H., Wingender,E. and Werner,T. (1995) Matlnd and matlnspector: new fast and versatile tools for detection of consensus matches in nucleotide sequence data. *Nucleic Acids Res.*, **23**, 4878–4884.
43. Uhlén,M., Fagerberg,L., Hallström,B.M., Lindskog,C., Oksvold,P., Mardinoglu,A., Sivertsson,Å., Kampf,C., Sjöstedt,E., Asplund,A. *et al.* (2015) Tissue-based map of the human proteome. *Science*, **347**, 1260419.
44. Hebbard,L. and George,J. (2011) Animal models of nonalcoholic fatty liver disease. *Nat. Rev. Gastroenterol. Hepatol.*, **8**, 35–44.
45. Berasain,C. and Avila,M.A. (2014) Amphiregulin. *Semin. Cell Dev. Biol.*, **28**, 31–41.
46. Zhou,V.W., Goren,A. and Bernstein,B.E. (2011) Charting histone modifications and the functional organization of mammalian genomes. *Nat. Rev. Genet.*, **12**, 7–18.
47. Calo,E. and Wysocka,J. (2013) Modification of enhancer chromatin: what, how, and why? *Mol. Cell*, **49**, 825–837.
48. Czaja,M.J. (2010) JNK regulation of hepatic manifestations of the metabolic syndrome. *Trends Endocrinol. Metab.*, **21**, 707–713.
49. Seki,E., Brenner,D.A. and Karin,M. (2012) A liver full of JNK: signaling in regulation of cell function and disease pathogenesis, and clinical approaches. *Gastroenterol.*, **143**, 307–320.
50. Zeke,A., Misheva,M., Reményi,A. and Bogoyevitch,M.A. (2016) JNK signaling: regulation and functions based on complex protein-protein partnerships. *Microbiol. Mol. Biol. Rev.*, **80**, 793–835.
51. Meng,Z., Moroishi,T. and Guan,K.L. (2016) Mechanisms of hippo pathway regulation. *Genes Dev.*, **30**, 1–17.
52. Campbell,C.T., Kolesar,J.E. and Kaufman,B.A. (2012) Mitochondrial transcription factor a regulates mitochondrial transcription initiation, DNA packaging, and genome copy number. *Biochim. Biophys. Acta - Gene Regul. Mech.*, **1819**, 921–929.
53. Schlegelmilch,K., Mohseni,M., Kirak,O., Pruszak,J., Rodriguez,J.R., Zhou,D., Kreger,B.T., Vasioukhin,V., Avruch,J., Brummelkamp,T.R. *et al.* (2011) Yap1 acts downstream of α-catenin to control epidermal proliferation. *Cell*, **144**, 782–795.
54. Melber,A. and Haynes,C.M. (2018) UPR mt regulation and output: a stress response mediated by mitochondrial-nuclear communication. *Cell Res.*, **28**, 281–295.
55. Münch,C. and Harper,J.W. (2016) Mitochondrial unfolded protein response controls matrix pre-RNA processing and translation. *Nature*, **534**, 710–713.
56. Fu,Z., Ye,J., Dean,J.W., Bostick,J.W., Weinberg,S.E., Xiong,L., Oliff,K.N., Chen,Z.E., Avram,D., Chandel,N.S. *et al.* (2019) Requirement of mitochondrial transcription factor a in tissue-resident regulatory t cell maintenance and function. *Cell Rep.*, **28**, 159–171.
57. Vierbuchen,T., Ling,E., Cowley,C.J., Couch,C.H., Wang,X., Harmin,D.A., Roberts,C.W.M. and Greenberg,M.E. (2017) AP-1 transcription factors and the BAF complex mediate signal-dependent enhancer selection. *Mol. Cell*, **68**, 1067–1082.
58. Galli,G.G., Carrara,M., Yuan,W.C., Valdes-Quezada,C., Gurung,B., Pepe-Mooney,B., Zhang,T., Geeven,G., Gray,N.S., de Laat,W. *et al.* (2015) YAP drives growth by controlling transcriptional pause release from dynamic enhancers. *Mol. Cell*, **60**, 328–337.
59. Adelman,K., Kennedy,M.A., Nechaev,S., Gilchrist,D.A., Muse,G.W., Chinenov,Y. and Rogatsky,I. (2009) Immediate mediators of the inflammatory response are poised for gene activation through RNA polymerase II stalling. *Proc. Natl. Acad. Sci. USA*, **106**, 18207–18212.
60. Donner,A.J., Ebmeier,C.C., Taatjes,D.J. and Espinosa,J.M. (2010) CDK8 is a positive regulator of transcriptional elongation within the serum response network. *Nat. Struct. Mol. Biol.*, **17**, 194–201.
61. Gutierrez,L.S. and Gutierrez,J. (2021) Thrombospondin 1 in metabolic diseases. *Front. Endocrinol. (Lausanne)*, **12**, 638536.
62. Zaiss,D.M.W., Gause,W.C., Osborne,L.C. and Artis,D. (2015) Emerging functions of amphiregulin in orchestrating immunity, inflammation, and tissue repair. *Immunity*, **42**, 216–226.
63. Busser,B., Sancey,L., Brambilla,E., Coll,J.L. and Hurbin,A. (2011) The multiple roles of amphiregulin in human cancer. *Biochim. Biophys. Acta - Rev. Cancer*, **1816**, 119–131.
64. Coppé,J.P., Patil,C.K., Rodier,F., Sun,Y., Muñoz,D.P., Goldstein,J., Nelson,P.S., Desprez,P.Y. and Campisi,J. (2008) Senescence-associated secretory phenotypes reveal cell-nonautonomous functions of oncogenic RAS and the p53 tumor suppressor. *PLoS Biol.*, **6**, 2853–2868.
65. Kuilman,T. and Peeper,D.S. (2009) Senescence-messaging secretome: SMS-ing cellular stress. *Nat. Rev. Cancer*, **9**, 81–94.
66. Wiley,C.D., Velarde,M.C., Lecot,P., Liu,S., Sarnoski,E.A., Freund,A., Shirakawa,K., Lim,H.W., Davis,S.S., Ramanathan,A. *et al.* (2016) Mitochondrial dysfunction induces senescence with a distinct secretory phenotype. *Cell Metab.*, **23**, 303–314.